(Received 24 April 2024, Accepted 16 July 2024, Scheduled 23 July 2024)

Convex Optimization-Based Linear and Planar Array Pattern Nulling

Tong Van Luyen[1,*], Nguyen Van Cuong[1], and Phan Dang Hung[2]

[1] *Faculty of Electronic Engineering, Hanoi University of Industry, Hanoi, Vietnam*
[2] *Information Technology Center, Hanoi University of Industry, Hanoi, Vietnam*

ABSTRACT: In the landscape of wireless communication, smart antennas, or adaptive array antennas, have emerged as vital components, offering heightened gains and spectral efficiency in advanced communication systems such as 5G and beyond. However, augmenting network coverage, capacity, and quality of service remains a pressing concern amid advancing communication technologies and escalating user demands. Array antennas with reduced sidelobe levels, high directivity, and increased beam steering capabilities are sought after to address these challenges. This paper explores convex optimization as a potent tool for array synthesis problems, offering robust performance and solution efficiency. By formulating optimization problems as convex programming, sidelobe reduction challenges can be efficiently addressed. The paper presents a comprehensive investigation into convex optimization-based approaches for array pattern nulling, assessing their performance and computational efficiency in various scenarios. Numerical examples demonstrate the efficacy of the proposed methods in maintaining the main lobe, controlling sidelobe levels, and placing nulls at interfering directions, thereby advancing the state-of-the-art in smart antenna technology.

1. INTRODUCTION

In the realm of wireless communication, antennas have long been integral components, finding extensive utility across various domains including radar systems, signal processing, and telecommunications. The advent of smart antennas, also referred to as adaptive array antennas, has garnered significant attention in contemporary technological landscapes owing to their capacity of providing heightened gains and spectral efficiency [1]. Equipped with adaptive beamforming and beam steering capabilities [2], smart antennas have become indispensable components in advanced communication systems like the fifth generation (5G), beyond 5G, and satellite communication systems [3, 4]. However, as wireless communication technologies continue to advance and user demands escalate, a pressing need to augment network coverage, capacity, and quality of service arises. Consequently, considerable efforts are being directed toward exploring array antennas characterized by reduced sidelobe level (SLL), high directivity, high gain, and increased beam steering capabilities [5]. It is imperative for antenna arrays to maintain a narrow first null beamwidth (FNBW) or narrow half-power beamwidth (HPBW) to achieve high directivity, ensuring optimal radiation patterns and minimizing interference with other systems operating in the same frequency band [6]. However, designing an antenna array with low SLL, null control, and narrow directivity presents a formidable challenge, as arrays with low SLL do not inherently exhibit narrow directivity, and vice versa.

Numerous methodologies for efficient array pattern synthesis have been proposed over the past few decades. For instance, the classical Chebyshev method enables the synthesis of linear arrays with specified sidelobe levels, while iterative Fourier transform methods, as detailed in [7], facilitate the synthesis of planar arrays with low sidelobe patterns. However, these methods are restricted to synthesizing uniform arrays with identical elements. Other synthesis methods based on adaptive array theory, as described in [8], have greater flexibility in array geometry but may lack precise control over array patterns according to desired specifications. Additionally, global optimization methods, like grey wolf optimizers [9, 10], bat algorithms [11], and particle swarm optimization [12], have been employed for array synthesis problems. While these methods offer flexibility and yield satisfactory results for small problem sizes, their computational complexity escalates significantly as problem sizes increase.

Planar arrays, with their ability to facilitate two-dimensional direction of arrival (2D-DOA) estimation, offer significant advantages over linear arrays in advanced communication systems. The flexibility and enhanced resolution provided by these arrays make them particularly appealing for a wide range of applications [13]. For instance, nonuniform linear arrays generate difference coarrays that enable large degrees of freedom and reduced mutual coupling, which are beneficial for DOA estimation. Enhanced and generalized coprime arrays have been shown to provide more uniform degrees of freedom than previous coprime arrays by coarray extension and hole filling, resulting in superior performance in subspace-based algorithms. This advanced capability positions planar arrays as a superior choice in scenarios requiring precise and efficient direction finding [14].

* Corresponding author: Tong Van Luyen (luyentv@haui.edu.vn).

Moreover, multiple-input and multiple-output sparse electromagnetic vector sensor arrays have brought new perspectives to signal processing due to their flexibility and higher resolution. In a monostatic multiple-input and multiple-output system, angle estimation using arbitrary geometry electromagnetic vector sensor arrays can be improved with parallel factor-based algorithms, achieving superresolution estimation with low computational complexity. This method leverages the natural multidimensional structure of the array output, rearranging it into a parallel factor model and applying vector cross-product and phase compensation for refined estimation. Such techniques further underscore the advantages of using sophisticated array configurations in modern communication systems [15].

In recent years, convex optimization has emerged as a potent tool for array synthesis problems. By formulating optimization problems as convex programming, sidelobe reduction challenges can be efficiently addressed. Leveraging interior point-based optimization tools such as the CVX toolbox [16], optimal solutions can be readily obtained [17]. The key advantages of convex optimization for array synthesis lie in its ability to handle arbitrary array configurations and adequately account for element patterns or mutual coupling effects [18, 19]. Furthermore, convex optimization algorithms can effectively address non-convex array synthesis problems by introducing appropriate approximations, relaxations, or iterative optimization approaches [20, 21]. This renders convex optimization a highly promising solution method for array synthesis problems, with robust performance and excellent solution efficiency [22].

In the synthesis of uniformly spaced arrays, two main optimization objectives are typically pursued. Firstly, sidelobe level and/or null depth level (NDL) minimization can be achieved by adjusting weight coefficients with a fixed number of antennas, employing nature-inspired computational techniques or convex optimization approaches [12, 23]. Secondly, the number of antennas required to produce a desired beam pattern can be minimized by adjusting weight coefficients. The matrix pencil method, introduced in [24], offers a solution for synthesizing sparse arrays. Rooted in signal processing parameter estimation, this method eliminates the need for iterative procedures, resulting in a significant reduction in the number of elements within a short time frame. However, it determines the minimum number of elements required to fit a given reference pattern in both amplitude and phase accurately. Consequently, there is no guarantee that the obtained number of elements is the absolute minimum. Non-evolutionary algorithms [25], such as linear programming and compressive sensing algorithms, form the bulk of alternative approaches. These approaches enable a significant reduction in the number of elements while ensuring the creation of desired gain patterns across the aperture.

While many global optimization methods entail high computational intensity, leading to increased costs with larger problem sizes, convex optimization presents an efficient compromise between analytical methods and numerical techniques. This paper employs the convex optimization approach to optimize the radiation patterns of linear and planar arrays. Initially, fully perturbed weight coefficients are optimized using the L2 norm, ensuring the preservation of the main lobe while nulls are strategically placed in interfering directions. Moreover, there exists a pressing need for an optimized method capable of perturbing precisely the required number of elements to efficiently place the necessary nulls. In addition to weight coefficients, the optimization of the minimum number of perturbed elements is carried out using the L1 norm. The solution's sparsity is further enhanced through the iterative reweighted L1 norm algorithm. By removing elements with weights approximately equal to zero, this approach facilitates the efficient placement of required nulls with the exact number of perturbed elements necessary.

The paper proceeds as follows. Section 2 formulates the array pattern nulling problem, followed by Section 3 which outlines pattern nulling approaches based on convex optimization for synthesizing array patterns amidst interfering signals. The performances of the two regularization methods, capable of imposing nulls towards interfering directions while maintaining the main lobe, are assessed in Section 4. Finally, concluding remarks are provided in Section 5.

2. ARRAY PATTERN NULLING FORMULATION

Consider a uniform rectangular array (URA), a type of uniform planar array, of $M \times N$ half-wavelength dipoles as shown in Figure 1. The array pattern at (θ, ϕ) direction can be expressed as [26]:

$$\begin{aligned} P(\theta,\phi) &= EF(\theta,\phi)\, AF(\theta,\phi) \\ &= EF(\theta,\phi) \sum_{m=0}^{M-1} \sum_{n=0}^{N-1} w_{m,n} e^{j(m\psi_z + n\psi_y)}, \end{aligned} \tag{1}$$

where:

- EF and AF are the element factor and the array factor of the dipole (θ, ϕ), respectively.

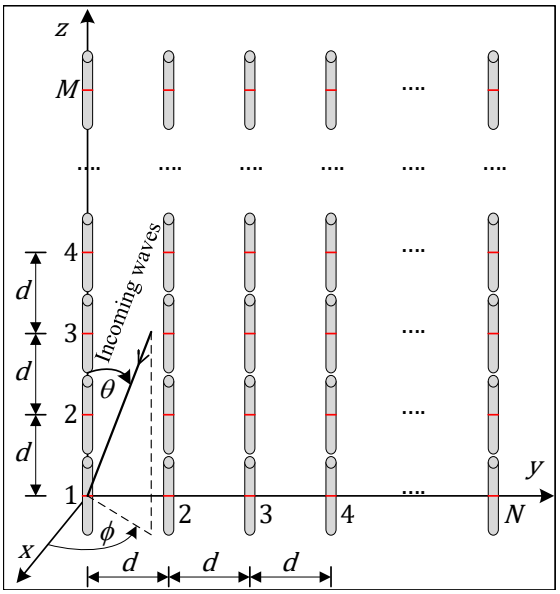

FIGURE 1. The uniform rectangular array with $M \times N$ elements.

- $EF(\theta,\phi) = \dfrac{\cos\left(\frac{\pi}{2}\cos(\theta)\right)}{\sin(\theta)}$.
- $\psi_z = \kappa d_z \cos(\theta)$; $\psi_y = \kappa d_y \sin(\theta)\sin(\phi)$; $\kappa = 2\pi/\lambda$.
- $w_{m,n} = a_{m,n}e^{j\delta_{m,n}}$ is the complex weight of the $(m,n)^{th}$ element, where $a_{m,n}$ and $\delta_{m,n}$ are the amplitude and the phase, respectively.

The main lobe can be steered towards the direction (θ_0, ϕ_0) by setting the phase shift of the $(m,n)^{th}$ antenna element as:

$$\delta_{m,n} = -\kappa\left(md_z\cos(\theta_0) + nd_y\sin(\theta_0)\sin(\phi_0)\right). \quad (2)$$

The array pattern for URAs can be expressed in the matrix form as follows:

$$P(\theta,\phi) = EF(\theta,\phi)\,\mathbf{s}(\theta,\phi)\,\mathbf{w}, \quad (3)$$

where:

$$\mathbf{w} = [w_{0,0},\ldots,w_{M-1,N-1}]^T, \quad (4)$$

$$\mathbf{s}(\theta,\phi) = \left[e^{j(m_0\psi_z+n_0\psi_y)},\ldots,e^{j(m_{M-1}\psi_z+n_{N-1}\psi_y)}\right]. \quad (5)$$

In the same manner, the array pattern for the uniform linear array (ULA) in Figure 2 can be expressed as [26]:

$$P(\theta,\phi) = EF(\theta,\phi)\,\mathbf{s}(\theta,\phi)\,\mathbf{w}, \quad (6)$$

where: $\mathbf{s}(\theta,\phi)$ is the steering vector for ULAs, and $\mathbf{w}$ is the weight vector for ULAs.

$$\mathbf{w} = [w_0,\ldots,w_{N-1}]^T, \quad (7)$$

$$\mathbf{s}(\theta,\phi) = \left[e^{j(n_0\psi_y)},\ldots,e^{j(n_{N-1}\psi_y)}\right]. \quad (8)$$

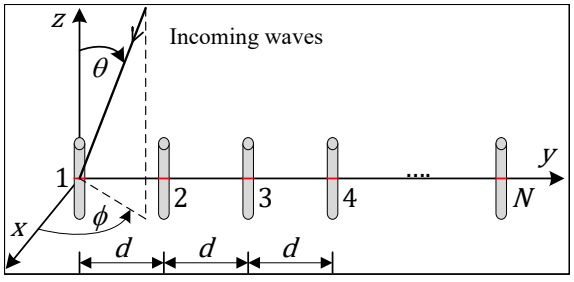

FIGURE 2. The uniform linear array with N elements.

To achieve the desired array pattern with K nulls in the directions (θ_k,ϕ_k), the pattern nulling problem with respect to $\mathbf{w}$ can be formulated as:

$$\begin{aligned} \max_{\mathbf{w}} \quad & P(\theta_0,\phi_0) \\ \text{s.t.} \quad & P(\theta_k,\phi_k) \le P_{\text{thr}} \quad \forall k = 1,\ldots,K, \end{aligned} \quad (9)$$

where: P_{thr} is the threshold for the desired null-depth level.

3. CONVEX OPTIMIZATION-BASED PATTERN NULLING

3.1. Pattern Nulling with L2 Norm

Achieving an optimal antenna pattern, which maintains the main beam integrity while effectively controlling sidelobes and positioning nulls at interference points, poses a significant challenge. In light of this complexity, a strategy built upon reference patterns that uphold the main lobe and sidelobe characteristics may offer a less formidable approach. Essentially, this entails forming optimal weights based on reference weights to ensure the preservation of desired pattern attributes. Hence, the optimal weight vector for addressing problem (9) through a convex optimization-based approach is represented as follows:

$$\mathbf{w}_{\text{o}} = \mathbf{w}_{\text{ref}} - \boldsymbol{\Delta}, \quad (10)$$

where:

- $\mathbf{w}_{\text{o}}$: the optimal weight vector.
- $\mathbf{w}_{\text{ref}}$: the reference weight vector, such as weights based on the Chebyshev method.
- $\boldsymbol{\Delta}$: the perturbation of the weight vector.

The optimized pattern with imposed nulls, maintained main lobe, and suppressed sidelobes is then presented as:

$$\begin{aligned} P_{\text{o}}(\theta,\phi) &= EF(\theta,\phi)\,\mathbf{s}(\theta,\phi)\,\mathbf{w}_{\text{o}} \\ &= EF(\theta,\phi)\,\mathbf{s}(\theta,\phi)\,(\mathbf{w}_{\text{ref}} - \boldsymbol{\Delta}), \end{aligned} \quad (11)$$

$$\begin{aligned} &\Leftrightarrow P_{\text{o}}(\theta,\phi) \\ &= EF(\theta,\phi)\,\mathbf{s}(\theta,\phi)\,\mathbf{w}_{\text{ref}} - EF(\theta,\phi)\,\mathbf{s}(\theta,\phi)\,\boldsymbol{\Delta}, \end{aligned} \quad (12)$$

$$\begin{aligned} &\Leftrightarrow P_{\text{o}}(\theta,\phi) \\ &= EF(\theta,\phi)\,AF_{\text{ref}}(\theta,\phi) - EF(\theta,\phi)\,\mathbf{s}(\theta,\phi)\,\boldsymbol{\Delta}. \end{aligned} \quad (13)$$

Specify the number of antennas as N_a, where $N_a = N$ for ULAs, and $N_a = M \times N$ for URAs. To impose K nulls towards interference directions, denoted by $k = 1,\ldots,K$, with NDLs equal to or less than S_{dB} from the main lobe's peak, the resulting equations are formulated as follows:

$$\|\mathbf{v}_{\text{ref}} - \mathbf{S}\boldsymbol{\Delta}\|_2 \le Thr, \quad (14)$$

where:

$$\mathbf{S} = \begin{bmatrix} s(\theta_1,\phi_1)_1 & \cdots & s(\theta_1,\phi_1)_{N_a} \\ \vdots & \ddots & \vdots \\ s(\theta_K,\phi_K)_1 & \cdots & s(\theta_K,\phi_K)_{N_a} \end{bmatrix}, \quad (15)$$

$$\boldsymbol{\Delta} = [\Delta_1,\ldots,\Delta_{N_a}]^T, \quad (16)$$

$$\mathbf{v}_{\text{ref}} = [AF_{\text{ref}}(\theta_1,\phi_1),\ldots,AF_{\text{ref}}(\theta_K,\phi_K)]^T, \quad (17)$$

$$Thr = 10^{\frac{-S_{\text{dB}}+20\log_{10}(P_{\text{ref}}(\theta_0,\phi_0))}{20}}. \quad (18)$$

In (14), the L2 norm serves as a regularization term aimed at penalizing large values exceeding Thr. By incorporating the square of the L2 norm, optimization algorithms are encouraged to generate solutions featuring reduced radiation magnitudes, thereby mitigating overfitting and enhancing generalization. The null depth levels are constrained by (14); nonetheless, to minimize the deviation of optimal weights from the reference weights, it is essential to minimize $\boldsymbol{\Delta}$. Leveraging the properties of the L2 norm, the pattern nulling problem can be formulated as follows:

$$\begin{aligned} \min_{\boldsymbol{\Delta}} \quad & \|\boldsymbol{\Delta}\|_2 \\ \text{s.t.} \quad & \|\mathbf{v}_{\text{ref}} - \mathbf{S}\boldsymbol{\Delta}\|_2 - Thr \leq 0. \end{aligned} \tag{19}$$

The objective and constraint functions are both convex, rendering the problem amenable to a solution using the CVX toolbox [16] to derive the optimal weights for the desired pattern.

3.2. Pattern Nulling with L1 Norm

The pattern nulling approach utilizing the L2 norm effectively preserves the main lobe, sidelobe levels, and null depth levels. However, it does not guarantee the minimum number of antennas necessary to achieve the desired beam pattern. To adjust the minimum weight coefficients, it is imperative to determine the number of nonzero coefficients in $\boldsymbol{\Delta}$. This necessitates the design of a formulation for L1 minimization, which more equitably penalizes nonzero coefficients. An iterative algorithm is proposed, where each iteration tackles a convex optimization problem.

A collection of linear inequalities $\|\mathbf{v}_{\text{ref}} - \mathbf{S}\boldsymbol{\Delta}\|_2 \leq Thr$ is deemed feasible. Two heuristic methods are utilized to discover a sparse point that meets these inequalities. The conventional L1 norm heuristic, employed for locating a sparse solution $\boldsymbol{\Delta}$, is denoted as:

$$\begin{aligned} \min_{\boldsymbol{\Delta}} \quad & \|\boldsymbol{\Delta}\|_1 \\ \text{s.t.} \quad & \|\mathbf{v}_{\text{ref}} - \mathbf{S}\boldsymbol{\Delta}\|_2 - Thr \leq 0. \end{aligned} \tag{20}$$

The log-based heuristic is an iterative technique aimed at identifying a sparse solution by seeking a local optimal point for the problem.

$$\begin{aligned} \min_{\boldsymbol{\Delta}} \quad & \sum_{i=1}^{N_a} \log\left(\varepsilon + \Delta_i\right) \\ \text{s.t.} \quad & \|\mathbf{v}_{\text{ref}} - \mathbf{S}\boldsymbol{\Delta}\|_2 - Thr \leq 0, \end{aligned} \tag{21}$$

where ε represents a small threshold value, determining the proximity to zero. Due to the minimization of a concave function, this problem remains unsolvable as it does not meet the criteria for convexity. Nonetheless, a heuristic approach can be employed wherein the objective is linearized, solved, and iterated upon. Consequently, the pattern nulling problem utilizing the L1 norm transforms into a weighted L1-norm heuristic:

$$\begin{aligned} \min_{\boldsymbol{\Delta}} \quad & \left\|\boldsymbol{\gamma}^{\ell}\boldsymbol{\Delta}\right\|_1 \\ \text{s.t.} \quad & \|\mathbf{v}_{\text{ref}} - \mathbf{S}\boldsymbol{\Delta}\|_2 - Thr \leq 0. \end{aligned} \tag{22}$$

The simple iterative algorithm to solve the problem (22) is as follows:

Result: Optimal weight coefficients: $\mathbf{w}_{\text{o}}^{*} = \mathbf{w}_{\text{ref}} - \boldsymbol{\Delta}^{*}$.
Initialize parameters for antenna arrays;
Set $\ell = 0$; $\boldsymbol{\Delta}^{0} = \mathbf{1}_{N_a \times 1}$; $maxIter = 10$; $\varepsilon = 1e^{-7}$;
while $\ell \leq maxIter$ **do**
  Solve the problem (22) by CVX toolbox to obtain $\boldsymbol{\Delta}^{\ell}$:

$$\begin{aligned} \boldsymbol{\Delta}^{\ell} &= \arg\min \left\|\boldsymbol{\gamma}^{\ell}\boldsymbol{\Delta}\right\|_1 \\ \text{s.t.} \quad & \|\mathbf{v}_{\text{ref}} - \mathbf{S}\boldsymbol{\Delta}\|_2 - \text{Thr} \leq 0. \end{aligned} \tag{23}$$

  Update the vector $\boldsymbol{\gamma}^{\ell+1}$ based on the rule:

$$\boldsymbol{\gamma}^{\ell+1} = \frac{1}{\boldsymbol{\Delta}^{\ell} + \varepsilon}. \tag{24}$$

end

Algorithm 1: The algorithm for the pattern nulling problem with L1 norm.

The parameter $\varepsilon > 0$ is selected to ensure stability and prevent a zero value in $\boldsymbol{\Delta}^{\ell}$ from entirely hindering a nonzero estimate in the subsequent step. Employing an iterative algorithm to form the vector $\boldsymbol{\Delta}$ enables a progressively refined estimation of the locations of nonzero coefficients. While initial iterations may yield inaccurate signal estimates, the larger signal coefficients are typically discerned as nonzero. Subsequently, these identified locations are given less weight to enhance sensitivity in identifying the remaining small yet nonzero signal coefficients.

4. NUMERICAL RESULTS

In this section, to evaluate the effectiveness of the proposed approach, various numerical examples are provided. It is worth noting that all simulations were conducted using MATLAB Online 2023b on an Intel(R) Xeon(R) Platinum 8375C CPU. For consistency, default parameters were used for all examples unless otherwise stated:

- $N = 20$ for ULAs and $M = N = 20$ for URAs; $\theta = 90°$; $S_{\text{dB}} = 60$ dB;
- The reference weights, $\mathbf{w}_{\text{ref}}$, are computed using the Chebyshev method-based weights with the SLL of -30 dB.

In our approach, we utilized the SDPT3 solver, which is a primal-dual interior-point algorithm that follows the path-following paradigm. This solver is integrated into the CVX toolbox [16], facilitating the resolution of convex optimization problems. The CVX toolbox abstracts the underlying complexities of the algorithm, providing a high-level interface for defining and solving convex programs. Consequently, we do not include a detailed algorithm flowchart, as the focus is on the application of convex optimization techniques to array pattern synthesis. The integration with CVX allows for efficient and robust performance in calculating the amplitude and phase coefficients necessary for array pattern nulling.

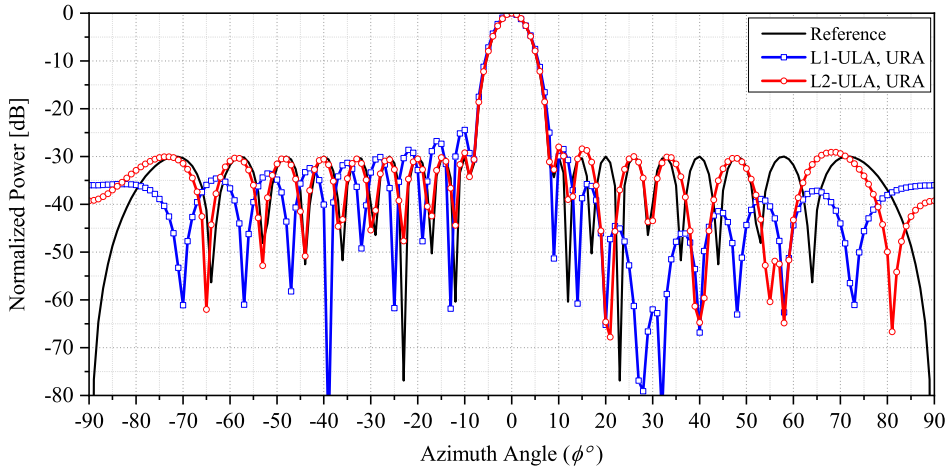

FIGURE 3. The normalized powers with three nulls at $[20°, 40°, 58°]$ and with $M = N = 20$.

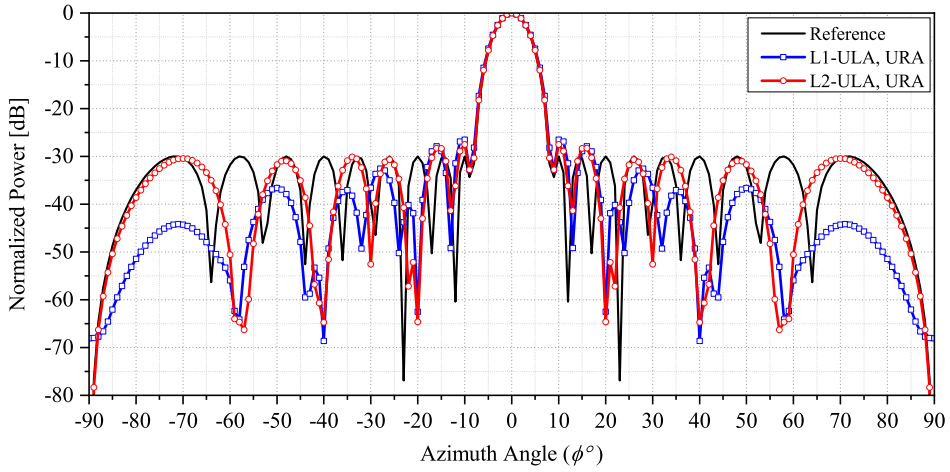

FIGURE 4. The normalized powers applied the amplitude-only technique with three nulls at $[20°, 40°, 58°]$ and with $M = N = 20$.

4.1. Pattern Nulling Ability

In this evaluation, we aim to verify the anti-interference capability of the proposed solution for both ULAs and URAs. Initially, we simulate interference occurring at angles $\phi = [20°, 40°, 58°]$ with $\phi_0 = 0°$. The optimized radiation pattern achieved by controlling complex weights, as depicted in Figure 3, demonstrates a remarkable preservation of the main beam and sidelobe levels, closely resembling the reference radiation pattern while effectively nulling interferences. Notably, the patterns for ULAs and URAs exhibit similar characteristics in the elevation cut plane at $\theta = 90°$, with the NDLs at $\phi = [20°, 40°, 58°]$ based on both L1 and L2 norms comfortably exceeding -60 dB, meeting the predefined threshold. However, it is worth noting that the two maximum SLLs in the L1 norm-based pattern are -24.5 dB and -26.8 dB. This disparity arises because the L1 norm-based approach also minimizes the number of antennas required to achieve the desired pattern, with the number of perturbed coefficients in $\boldsymbol{\Delta}$ set at 2, as summarized in Table 1.

In addition to controlling complex weights for pattern nulling, we also explore two approaches based solely on L1 and L2 norms to control amplitudes excited at each element. Using the same interfering directions as in the previous scenario, the results illustrated in Figure 4 reveal optimal patterns characterized by symmetric features and null points across the main lobe direction. However, it is noteworthy that the number of coefficients requiring adjustment is 5, higher than in the case of controlling complex weights.

TABLE 1. The number of perturbed elements.

Figure	L1-ULA	L1-URA
3	2	2
4	5	5
7	7	7

Figure 5 presents the amplitude and phase perturbations of the complex weights for a URA when three nulls are imposed at specific interference angles $[20°, 40°, 58°]$. The amplitude perturbation, shown on the left, demonstrates how the magnitude of the complex weights is adjusted across the array elements to achieve the desired nulling effect. The phase perturbation,

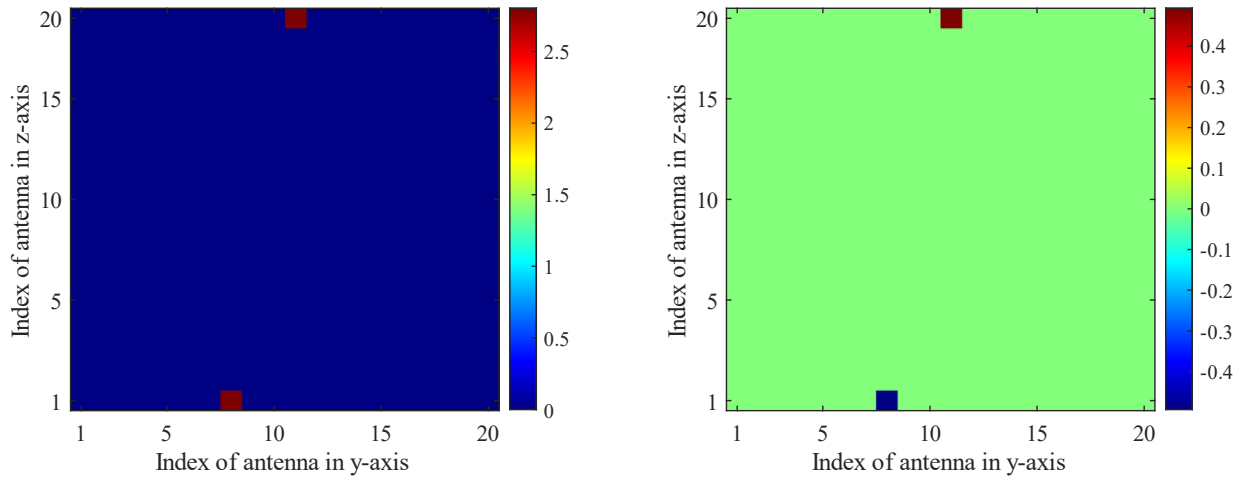

FIGURE 5. The amplitude (left) and phase (right) of the perturbation of the complex weights $\mathbf{\Delta}$ with three nulls at $[20°, 40°, 58°]$ and with $M = N = 20$.

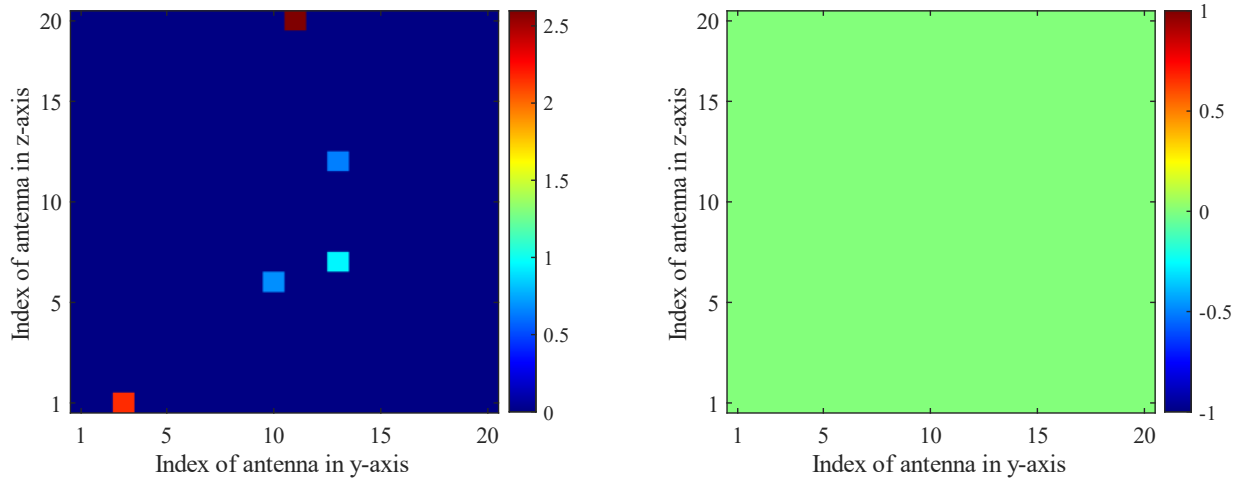

FIGURE 6. The amplitude (left) and phase (right) of the perturbation of the complex weights $\mathbf{\Delta}$ when applying the amplitude-only technique to impose three nulls at $[20°, 40°, 58°]$ and with $M = N = 20$.

shown on the right, illustrates the changes in the phase of the complex weights, which are crucial for precisely directing the nulls towards the interference angles. The amplitude perturbation plot reveals that the changes are not uniformly distributed, indicating that different elements in the array require different levels of adjustment to effectively impose the nulls. This non-uniformity is necessary to tailor the array's radiation pattern precisely. The phase perturbation plot further emphasizes the complexity of the adjustments needed. The phase shifts are designed to interfere destructively with the incoming signals from the interference directions, thereby nulling their effect. The specific patterns observed in both amplitude and phase perturbations highlight the sophisticated nature of the optimization process and its ability to fine-tune the array's response to achieve the desired performance.

Figure 6 illustrates the amplitude and phase perturbations of the complex weights for a URA using the amplitude-only technique to impose three nulls at the interference angles $[20°, 40°, 58°]$. Unlike the previous figure, the amplitude-only technique focuses primarily on adjusting the magnitude of the complex weights while keeping the phase adjustments minimal. In the amplitude perturbation plot (left), the adjustments in the magnitude of the complex weights are more pronounced compared to the phase perturbation plot. This indicates that the amplitude-only technique relies heavily on altering the power distribution across the array elements to achieve the nulling effect. The adjustments are strategically distributed to maximize the nulling effect without significantly altering the overall radiation pattern of the array. The phase perturbation plot (right), although still present, shows less variation compared to Figure 5. This suggests that the phase adjustments are secondary in this technique and serve to fine-tune the nulling effect achieved primarily through amplitude adjustments.

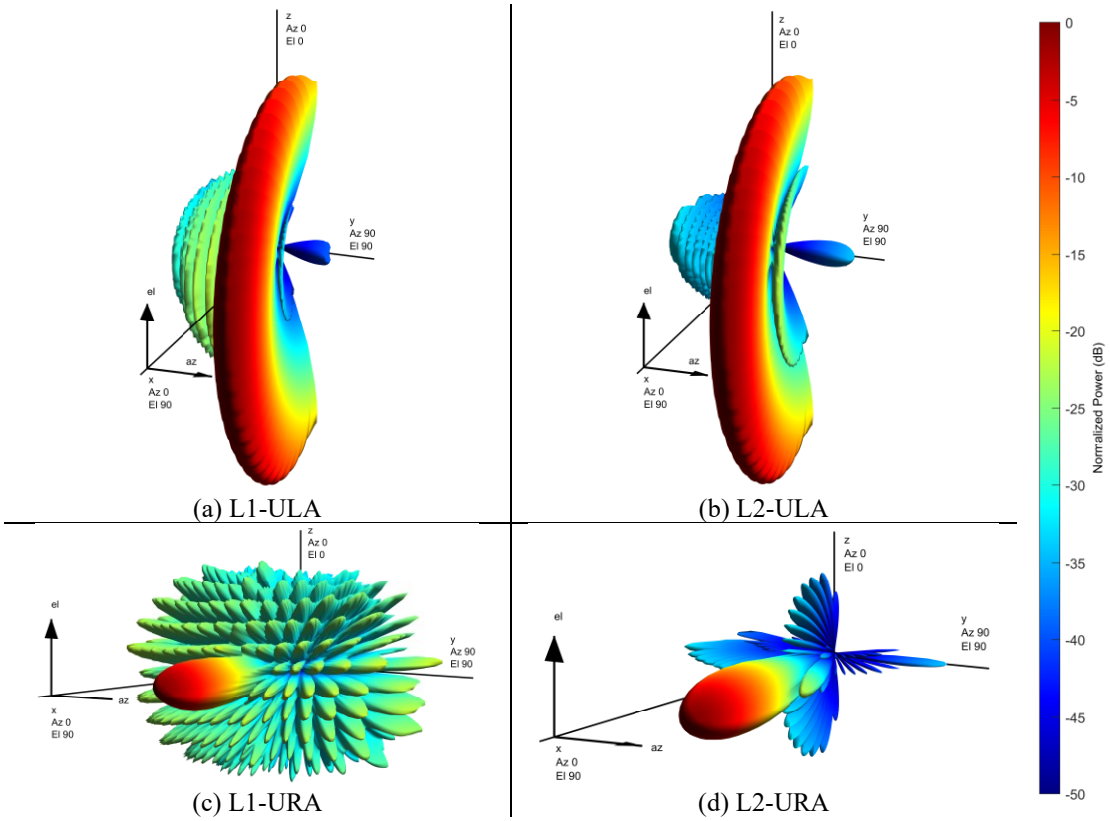

(a) L1-ULA (b) L2-ULA

(c) L1-URA (d) L2-URA

FIGURE 7. The 3D normalized patterns with a broad null from 30° to 60° and with $M = N = 20$.

The comparison between Figures 5 and 6 underscores the effectiveness of different nulling strategies. While the full complex weight perturbation (amplitude and phase) provides a more comprehensive adjustment mechanism, the amplitude-only technique offers a simpler yet effective approach for imposing nulls. The choice between these methods depends on the specific requirements of the application and the computational resources available.

To better visualize sidelobe suppression ability while imposing nulls in 3D space, we examine the scenario with interferences at $\phi = 30^\circ \rightarrow 60^\circ$ and $\phi_0 = 10^\circ$, as depicted in Figure 7. For ULAs, the L2 norm-based approach demonstrates superior sidelobe suppression compared to the L1 norm-based approach, with the latter exhibiting higher sidelobe levels above -30 dB. Nonetheless, both approaches effectively achieve null depths exceeding -60 dB. In the case of URAs, significant differences emerge between the two approaches. While the L1 norm-based approach generates numerous sidelobes above -30 dB, the L2 norm-based approach retains nearly all characteristics of the reference pattern, including the main lobe and sidelobes. Both approaches can achieve NDLs meeting the threshold; however, the L1 norm-based approach struggles to control SLLs due to its requirement to minimize the number of perturbed coefficients, presenting a tradeoff. With 7 nonzeros in $\boldsymbol{\Delta}$, the L1 norm-based approach contrasts with the 400 nonzeros in the L2 norm-based approach.

Furthermore, the cumulative distribution function (CDF) versus SLLs for URAs, as depicted in Figure 8, showcases that approximately 80% of SLLs in the L1 norm-based pattern fall below -30 dB, compared to 99.8% for the L2 norm-based pattern. Despite this, the L2 norm-based approach effectively controls SLLs below -30 dB while ensuring that nulls are imposed at the interfering directions.

4.2. Robustness of Pattern Nulling Approaches

The previous section focused on investigating the ability to set nulls, maintain the main lobe, and control SLLs using both L1 and L2 norm-based approaches. However, the robustness of these approaches has not been explored. Therefore, this subsection delves into various scenarios to assess the performance of the L1 and L2 norm-based methods. For consistency, the default parameters set, unless otherwise specified, include the main lobe direction at $\phi_0 = 10^\circ$, interfering directions at $\phi = 30^\circ \rightarrow 60^\circ$ and $S_{dB} = 60$ dB.

Initially, we examine the number of coefficients that need adjustment when increasing the number of nulls and varying the NDL threshold S_{dB} for the L1 norm-based approach. Figures 9 and 10 illustrate the change in the number of coefficients in $\boldsymbol{\Delta}$ versus the number of nulls ranging from 1 to 31 across the $\phi = 30^\circ \rightarrow 90^\circ$ range and versus the threshold ranging from 40 to 100 dB. The number of coefficients increases proportionally with the number of nulls and the NDL threshold. For instance, to establish 10 null points within the $30^\circ \rightarrow 90^\circ$ range with $S_{dB} = 60$ dB, 6 elements require adjustment to achieve the desired pattern. Conversely, to impose nulls within the $30^\circ \rightarrow$

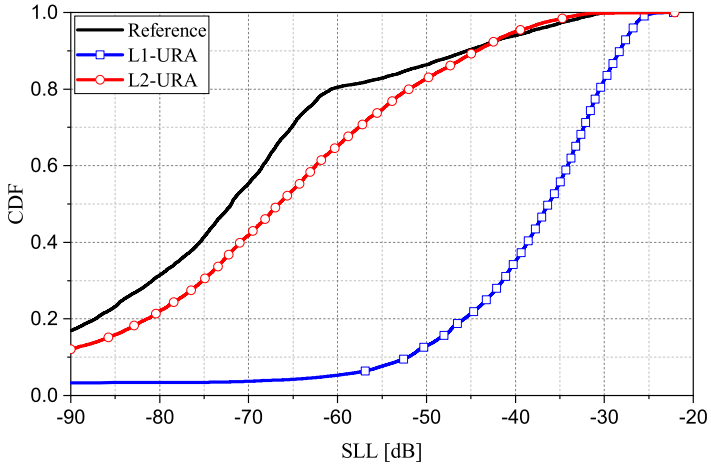

FIGURE 8. CDFs versus SLLs of URA pattern for the cases of a broad null with $\theta = 90^\circ$ and with $M = N = 20$.

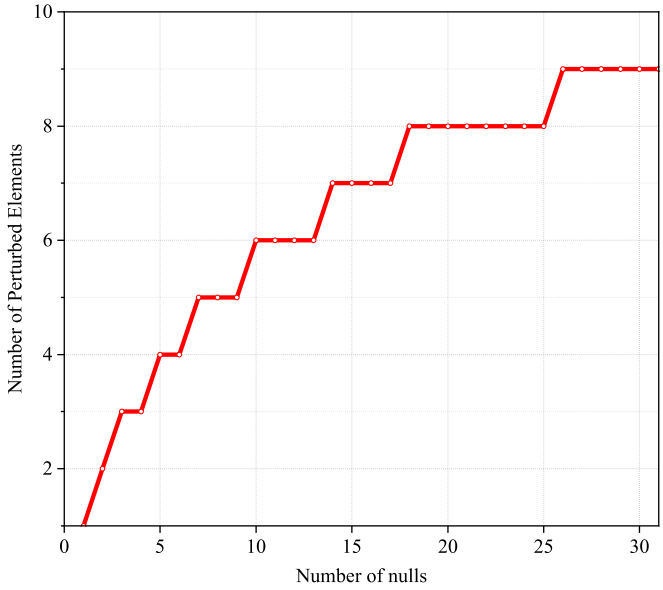

FIGURE 9. The number of perturbed elements versus the number of nulls ranging from 1 to 31 across the $30^\circ \rightarrow 90^\circ$ range with $M = N = 20$.

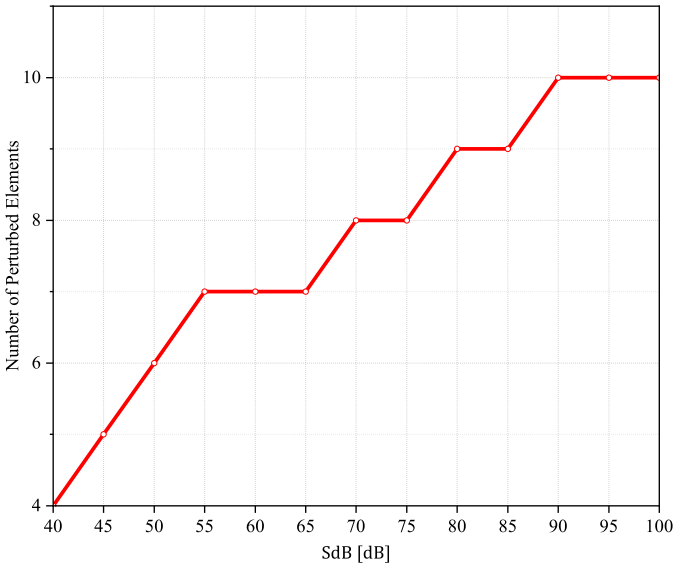

FIGURE 10. The number of perturbed elements versus the NDL threshold with a broad null from 30° to 60° and with $M = N = 20$.

TABLE 2. The computational time for two pattern nulling approaches.

Figure	L1-ULA-Time (s)	L1-URA-Time (s)	L2-ULA-Time (s)	L2-URA-Time (s)
3	2.9778	3.7275	0.2522	0.2579
4	2.6557	2.7518	0.2471	0.2496
7	3.4358	5.7309	0.3157	0.3536

60° range with $S_{dB} = 90$ dB, 10 elements must be adjusted relative to the reference weight vector.

Next, we examine computational time across different scenarios. Table 2 presents the time consumed by the L1 and L2 norm-based approaches for ULAs and URAs to optimize weights for patterns in Figures 3, 4, and 7. The L2 norm-based approach takes approximately 0.25 seconds to impose three nulls and below 0.36 seconds to impose a range of nulls from 30 to 60. Conversely, the L1 norm-based approach consumes roughly about 10 to 16 times more time than the L2 norm-based approach for the scenarios in Figures 3, 4, and 7. This disparity arises because the L1 norm-based approach requires iterations to minimize the number of nonzero coefficients.

Additionally, we investigate computational time in scenarios involving changes in the threshold across the $40 \rightarrow 100$ range with $\phi_0 = 10^\circ$ in Figure 11 and interfering directions at $\phi = 30^\circ \rightarrow 60^\circ$ in Figure 12. Utilizing URAs requires more time than using ULAs due to the greater number of coeffi-

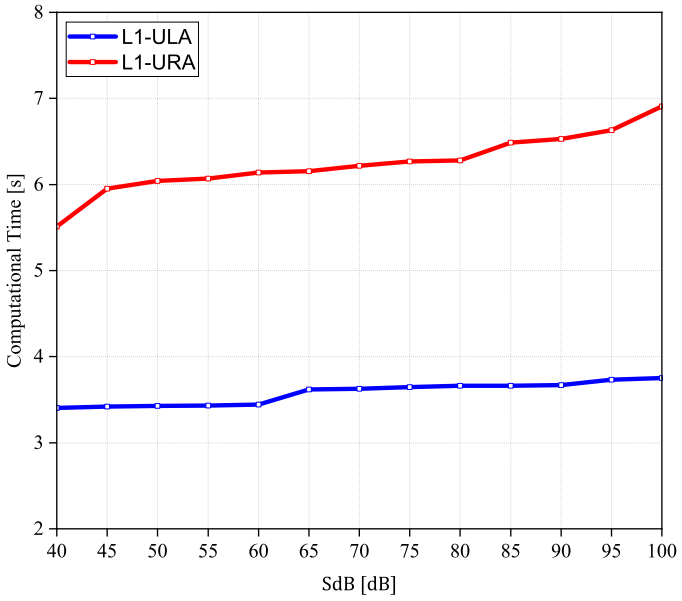

FIGURE 11. The computational time versus S_{dB} for ULAs with a broad null from 30° to 60° and with $N = 20$.

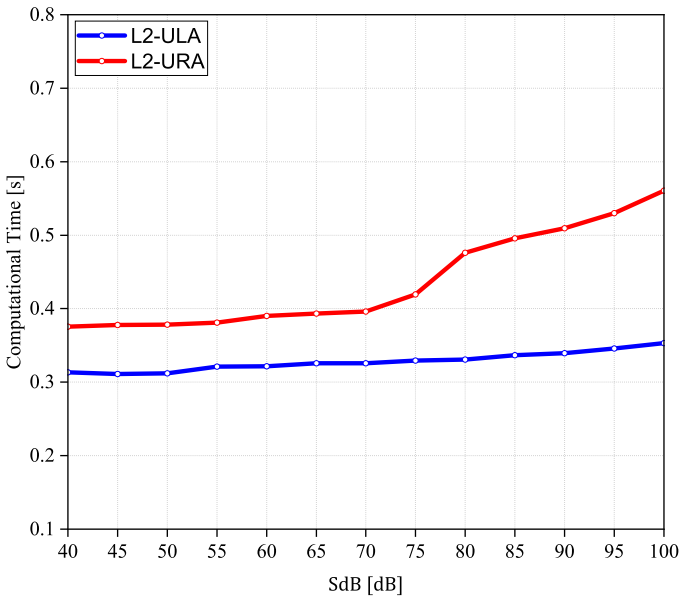

FIGURE 12. The computational time versus S_{dB} for URAs with a broad null from 30° to 60° and with $M = N = 20$.

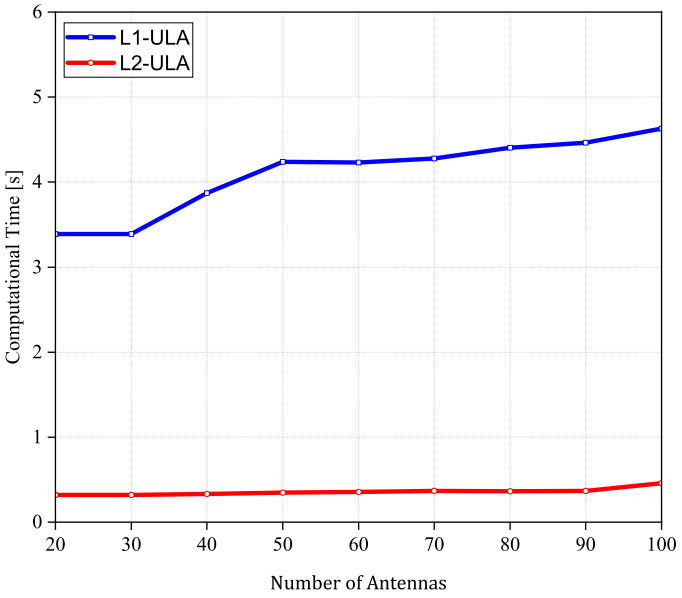

FIGURE 13. The computational time versus the number of antennas for ULAs with a broad null from 30° to 60°.

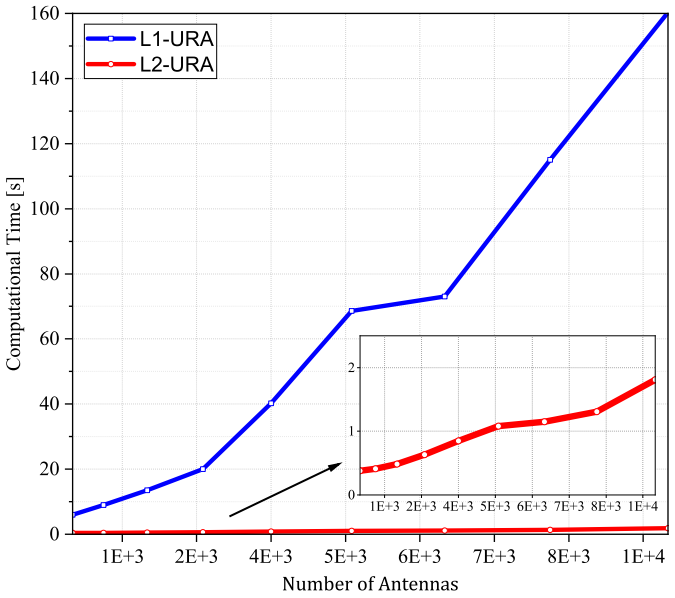

FIGURE 14. The computational time versus the number of antennas for URAs with a broad null from 30° to 60°.

cients requiring optimization, with deeper nulls also necessitating longer computational times. The L2 norm-based approach outperforms the L1 norm-based approach in terms of computational efficiency because it does not iterate to minimize the number of nonzero coefficients. For example, while the L2 norm-based approach for ULAs requires only about 0.3 seconds, the L1 norm-based approach requires approximately 3.5 seconds to find the optimized solutions.

Moreover, computational time is considered in scenarios involving an increase in the number of antennas, as depicted in Figures 13 and 14. As the number of antennas increases, the time consumed also increases. For ULAs, the L2 norm-based approach requires no more than 0.5 seconds to obtain optimized solutions within the $20 \rightarrow 100$ antenna range, while the L1 norm-based approach necessitates 3 to 5 seconds. For URAs, although the array comprises up to 1000 elements, the L2 norm-based approach requires no more than 2 seconds, whereas the L1 norm-based approach demands significantly more time to acquire solutions.

5. CONCLUSION

In this study, we have explored convex optimization-based approaches for array pattern nulling, addressing the critical need

for enhancing network coverage, capacity, and quality of service in wireless communication systems. Leveraging convex optimization, we have demonstrated the ability to efficiently address sidelobe reduction challenges and optimize array radiation patterns, even in the presence of interfering signals. Numerical examples have showcased the efficacy of the proposed methods in maintaining the main lobe, controlling sidelobe levels, and strategically placing nulls at interfering directions. Through comprehensive performance assessments and computational analyses, we have established the robustness and efficiency of convex optimization in array synthesis problems. These findings underscore the potential of convex optimization as a powerful solution method for advancing smart antenna technology and meeting the evolving demands of wireless communication networks.

ACKNOWLEDGEMENT

This research is supported by Hanoi University of Industry [Grant number: 25-2023-RD/HĐ-ĐHCN].

REFERENCES

[1] Liang, S., Z. Fang, G. Sun, Y. Liu, G. Qu, and Y. Zhang, "Sidelobe reductions of antenna arrays via an improved chicken swarm optimization approach," *IEEE Access*, Vol. 8, 37 664–37 683, 2020.

[2] Cheng, Y.-F., X. Ding, W. Shao, and C. Liao, "A high-gain sparse phased array with wide-angle scanning performance and low sidelobe levels," *IEEE Access*, Vol. 7, 31 151–31 158, 2019.

[3] Guo, Y. J. and R. W. Ziolkowski, *Advanced Antenna Array Engineering for 6G and Beyond Wireless Communications*, John Wiley & Sons, 2021.

[4] Jiang, W. and F.-L. Luo, *6G Key Technologies: A Comprehensive Guide*, John Wiley & Sons, 2022.

[5] Duong, T. Q., *Real Time Convex Optimisation for 5G Networks and Beyond*, Institution of Engineering and Technology (IET), 2021.

[6] Wang, H., C. Liu, H. Wu, B. Li, and X. Xie, "Optimal pattern synthesis of linear array and broadband design of whip antenna using grasshopper optimization algorithm," *International Journal of Antennas and Propagation*, Vol. 2020, No. 1, 5904018, 2020.

[7] Wang, X.-K., Y.-C. Jiao, and Y.-Y. Tan, "Synthesis of large thinned planar arrays using a modified iterative fourier technique," *IEEE Transactions on Antennas and Propagation*, Vol. 62, No. 4, 1564–1571, 2014.

[8] Hoang, K. M., L. V. Tong, and C. V. Nguyen, "A null synthesis technique-based beamformer for uniform rectangular arrays," in *2022 International Conference on Advanced Technologies for Communications (ATC)*, 13–17, Hanoi, Vietnam, 2022.

[9] Trang, L. T., N. V. Cuong, and T. V. Luyen, "Interference suppression approaches utilizing phase-only control and metaheuristic algorithms: A comparative study," in *International Conference on Ad Hoc Networks*, 65–85, 2023.

[10] Indumathi, G. and S. N. Rani, "Hybrid Grey Wolf Optimization with Cuckoo Search-based optimal channel estimation for energy efficient massive multiple input multiple output," *International Journal of Communication Systems*, Vol. 35, No. 7, e5106, 2022.

[11] Tong, L. and C. Nguyen, "An effective beamformer for interference suppression without knowing the direction," *International Journal of Electrical and Computer Engineering (IJECE)*, Vol. 13, No. 1, 601–610, 2023.

[12] Van Luyen, T., N. V. Cuong, and T. V. B. Giang, "Convex optimization-based sidelobe control for planar arrays," in *2023 IEEE Statistical Signal Processing Workshop (SSP)*, 304–308, Hanoi, Vietnam, 2023.

[13] Aboumahmoud, I., A. Muqaibel, M. Alhassoun, and S. Alawsh, "A review of sparse sensor arrays for two-dimensional direction-of-arrival estimation," *IEEE Access*, Vol. 9, 92 999–93 017, 2021.

[14] Shi, J., F. Wen, Y. Liu, Z. Liu, and P. Hu, "Enhanced and generalized coprime array for direction of arrival estimation," *IEEE Transactions on Aerospace and Electronic Systems*, Vol. 59, No. 2, 1327–1339, 2023.

[15] Zhang, Z., J. Shi, and F. Wen, "Phase compensation-based 2D-DOA estimation for EMVS-MIMO radar," *IEEE Transactions on Aerospace and Electronic Systems*, Vol. 60, No. 2, 1299–1308, 2024.

[16] Grant, M. and S. Boyd, "CVX: Matlab software for disciplined convex programming, version 2.1," https://cvxr.com/cvx, Mar. 2014.

[17] Boyd, S. and L. Vandenberghe, *Convex Optimization*, Cambridge University Press, 2004.

[18] Tsui, K. M. and S. C. Chan, "Pattern synthesis of narrowband conformal arrays using iterative second-order cone programming," *IEEE Transactions on Antennas and Propagation*, Vol. 58, No. 6, 1959–1970, 2010.

[19] Zhang, Y.-X., Y.-C. Jiao, and L. Zhang, "Antenna array directivity maximization with sidelobe level constraints using convex optimization," *IEEE Transactions on Antennas and Propagation*, Vol. 69, No. 4, 2041–2052, 2021.

[20] Zhang, X., Z. He, X. Zhang, and W. Peng, "High-performance beampattern synthesis via linear fractional semidefinite relaxation and quasi-convex optimization," *IEEE Transactions on Antennas and Propagation*, Vol. 66, No. 7, 3421–3431, 2018.

[21] Lei, S., H. Hu, B. Chen, P. Tang, J. Tian, and X. Qiu, "An array position refinement algorithm for pencil beam pattern synthesis with high-order taylor expansion," *IEEE Antennas and Wireless Propagation Letters*, Vol. 18, No. 9, 1766–1770, 2019.

[22] Yang, F., S. Yang, Y. Chen, S. Qu, and J. Hu, "Efficient pencil beam synthesis in 4-D antenna arrays using an iterative convex optimization algorithm," *IEEE Transactions on Antennas and Propagation*, Vol. 67, No. 11, 6847–6858, 2019.

[23] Kha, H. M., T. V. Luyen, and N. V. Cuong, "An efficient beamformer for interference suppression using rectangular antenna arrays," *Journal of Communications*, Vol. 18, No. 2, 116–122, 2023.

[24] Gu, P., G. Wang, Z. Fan, and R. Chen, "An efficient approach for the synthesis of large sparse planar array," *IEEE Transactions on Antennas and Propagation*, Vol. 67, No. 12, 7320–7330, 2019.

[25] Pinchera, D., M. D. Migliore, F. Schettino, M. Lucido, and G. Panariello, "An effective compressed-sensing inspired deterministic algorithm for sparse array synthesis," *IEEE Transactions on Antennas and Propagation*, Vol. 66, No. 1, 149–159, 2018.

[26] Balanis, C. A., *Antenna Theory: Analysis and Design*, John Wiley & Sons, 2016.